JOURNAL OF CATALYSIS **166,** 67–74 (1997)
ARTICLE NO. CA971504

An XRD and TEM Investigation of the Structure of Alumina-Supported Ceria–Zirconia

M. H. Yao,* R. J. Baird,* F. W. Kunz,* and T. E. Hoost†,[1,2]

Physics Department and Chemical Engineering Department†, Ford Research Laboratories, Ford Motor Company, MD 3179 SRL, P.O. Box 2053, Dearborn, Michigan 48121-2053*

Received October 26, 1995; revised September 27, 1996; accepted October 30, 1996

Dispersed CeO_2–ZrO_2 is of interest as a thermally stable oxygen-storage component of automotive catalysts. Alumina-supported CeO_2–ZrO_2 samples were prepared by coimpregnation in order to maximize the interaction between Zr and Ce. The phases present, their particle sizes and the interactions among the phases of fresh, steam-aged and reduced samples were investigated by XRD and TEM. In the fresh samples, a particulate solid solution phase $Zr_xCe_{1-x}O_2$ of cubic symmetry was identified. However, the zirconium concentration of this particulate phase was found to be smaller than that expected from the Zr loading. This suggests the existence of finely dispersed zirconia on the Al_2O_3 surface. For the steam-aged samples, a second Ce–Zr oxide solid solution phase of higher Zr concentration and tetragonal symmetry was found in addition to the original CeO_2-based cubic solid solution. The appearance of this second phase may have resulted from sintering of the highly dispersed zirconia. The highly dispersed zirconia may also be responsible for preventing reaction between CeO_2 and the Al_2O_3 support, since $CeAlO_3$ was found only in high-temperature reduced samples without zirconia. The particle sizes of the various phases were measured by XRD and TEM. The particle size of the supported particulate phase decreased with increasing zirconium loading, but a discrepancy was noted between the XRD and the TEM results. This discrepancy is discussed in terms of compositional inhomogeneity in the $Zr_xCe_{1-x}O_2$ solid solution phase.

1. INTRODUCTION

The behavior of ceria and zirconia is of interest in view of their importance as additives or promoters in automotive catalysts. CeO_2 is known to enhance the CO oxidation activity of some catalysts (1), to promote low-temperature water–gas shift (2), to stabilize the noble metal dispersion (3), and to minimize the thermally induced sintering of alumina supports. However, the primary function of ceria in automotive catalysts is to provide oxygen storage capacity (OSC) in order to allow the catalyst to operate over a wider range of air/fuel ratios (4). It has been reported that adding ZrO_2 to CeO_2 increases OSC (5), and stabilizes CeO_2 particles against thermal sintering (6). While there have been extensive investigations (7–10) of the phase diagram of the ceramic system CeO_2–ZrO_2 because of its electroconductive and mechanical properties, the structure and phases of Al_2O_3 supported CeO_2–ZrO_2 and the interactions among these phases have not been reported. Also, the mechanism by which CeO_2–ZrO_2 enhances OSC is not well understood.

In this research, high-surface-area CeO_2–ZrO_2/Al_2O_3 samples were prepared by coimpregnation. The structure, size, phases, and interactions among the phases of the system were investigated by X-ray diffraction (XRD) and transmission electron microscopy (TEM) as a function of Zr loading and thermal treatment.

2. EXPERIMENTAL

Sample Preparation

A series of alumina-supported CeO_2–ZrO_2 samples was prepared as follows. Appropriate amounts of zirconium dinitrate oxide ($ZrO(NO_3)_2$, Johnson Matthey, 99.9985%) and cerium nitrate ($Ce(NO_3)_3 \cdot 6H_2O$, Johnson Matthey, 99.99%) were combined in several aqueous solutions. These solutions were used to coimpregnate Zr and Ce into defumed alumina (Degussa Alumina C, 100 m^2/g, precalcined at 600°C for 16 h) by the incipient-wetness technique. These preparations were dried at 120°C and calcined at 400°C for 4 h, resulting in the fresh samples. The Zr and Ce concentrations of the fresh samples were measured using a Siemens SRS303 sequential wavelength dispersive X-ray fluorescence spectrometer with a Cr X-ray tube operated at 40 kV and 30 mA. The nominal and measured concentrations of Ce and Zr are listed in Table 1. When the measured compositions are used in calculating the stoichiometry the subscript "m" is added to the mole fraction. Steam-aged samples were prepared by hydrothermal treatment (10% water/90% He, 1000°C, 24 h) of the fresh samples. Reduced samples were prepared by heating fresh samples in a flowing H_2/Ar mixture (Airco, 8.85%) at 15°C/min to 900°C, followed by cooling in H_2/Ar to room temperature. Table 2

[1] To whom correspondence should be addressed.
[2] FAX: (313) 594-2963. E-mail: thoost@ford.com.

0021-9517/97 $25.00

TABLE 1

Nominal and Measured Zr and Ce Concentration

Sample and nominal loading[a] $ZrO_2(\mu mol/g\text{-}Al_2O_3)CeO_2(\mu mol/g\text{-}Al_2O_3)/Al_2O_3$	Zr/Ce atomic ratio		X_m in[b] $Zr_xCe_{1-x}O_2$
	Nominal	Measured	
1. $ZrO_2(0)CeO_2(1500)/Al_2O_3$	0	0	0
2. $ZrO_2(150)CeO_2(1500)/Al_2O_3$	0.1	0.13	0.12
3. $ZrO_2(300)CeO_2(1500)/Al_2O_3$	0.2	0.22	0.19
4. $ZrO_2(750)CeO_2(1500)/Al_2O_3$	0.5	0.54	0.35
5. $ZrO_2(1500)CeO_2(1500)/Al_2O_3$	1.0	1.02	0.51
6. $ZrO_2(1500)CeO_2(0)/Al_2O_3$			1.0

[a] μMol of ceria or zirconia per gram of alumina.
[b] Based on measured Zr/Ce ratio, assuming complete incorporation of Zr and Ce into the solid-solution phase $Zr_xCe_{1-x}O_2$.

shows BET surface areas for the fresh and hydrothermally aged samples. Sample sizes of the reduced catalysts were too small to permit reliable surface area determination. BET surface areas were measured on a Micrometrics ASAP-2400 instrument.

X-Ray Diffraction

The X-ray diffraction patterns were acquired on a Scintag XDS-2000 diffractometer operated at 45 kV and 40 mA with Cu$K\alpha$ radiation ($\lambda = 1.5406$ Å) and a diffracted beam monochromator. Data processing (including background correction, $K\alpha_2$ stripping, peak identification, particle size analysis, and lattice refinement) was accomplished using the Scintag DMS software package. Due to the small particle sizes, the XRD peaks were extensively broadened, and some peaks overlapped. Peak positions and widths were resolved by profile fitting. The Pearson VII profile-shape function was used in the fitting. Average particle sizes were then estimated from X-ray line width broadening using the Scherrer equation [11]

$$\beta = \frac{K\lambda}{L_w \cos\theta}, \qquad [1]$$

where K is a constant taken as 0.94 in this study, λ is the X-ray wavelength, and β is the corrected peak width. In these experiments, the width is taken as the full width at half maximum intensity of the most intense and least overlapped peak assigned to a particular phase.

Since the changes of structure and lattice as a function of Zr/Ce ratio and temperature of treatment are subtle, an internal reference was used to ensure the accuracy of the peak positions. A small amount (<5%) of Si powder (NBS Standard Reference Material No. 640b) was mixed with the samples as the internal reference. Diffraction peak positions of unknown phases determined by profile fitting were corrected using the internal reference peaks. Lattice parameters of various phases were calculated using the lattice refinement procedure on the Scintag system and plotted as a function Zr/Ce ratio and thermal treatment. For the sake of clarity and simplicity of the figures, the XRD patterns shown in this paper were acquired without the internal reference standard. However, all results were calculated from XRD patterns recorded with the internal reference.

TABLE 2

BET Areas for Alumina-Supported Zirconia–Ceria after Hydrothermal Treatment[a]

Catalysts	BET surface area, m^2/g (at various aging times)		
	0 h	4 h	24 h
Al_2O_3	105	73	68
$ZrO_2(0)CeO_2(1500)/Al_2O_3$	79	56	51
$ZrO_2(150)CeO_2(1500)/Al_2O_3$	82	57	52
$ZrO_2(300)CeO_2(1500)/Al_2O_3$	83	56	52
$ZrO_2(750)CeO_2(1500)/Al_2O_3$	84	54	50
$ZrO_2(1500)CeO_2(1500)/Al_2O_3$	88	51	48
$ZrO_2(1500)CeO_2(0)/Al_2O_3$	105	63	59

[a] Steamed at 1000°C in 10 mol% H_2O in He.

Electron Microscopy

TEM observations were made on a JEOL JEM-2000FX microscope equipped with a Link AN10000 EDX spectrometer and a Gatan TV camera. CeO_2–ZrO_2/Al_2O_3 powders were supported on holey carbon film mounted on Cu grids. More than 100 particles for each sample were counted for particle size distribution measurement and average size calculation. It has been pointed out (12) that the volume-weighted average size measured by TEM should be comparable to the size calculated by the Scherrer equation. Simple average size, area-weighted average size, and volume-weighted average size were calculated from TEM

data using KleidaGraph on a Macintosh computer. The TEM procedure was given in previous paper (12).

3. RESULTS

The XRD patterns of fresh samples with different Zr loading are given in Fig. 1. Two phases were identified in each diffraction pattern of Fig. 1(a–c): γ-Al_2O_3 which was labeled A; and a phase which was indexed using cubic symmetry and labeled B. Also, the greater the Zr loading, the more the B peaks shifted to larger 2θ. Based on these observations combined with the fact that no Zr or Zr oxide particulate phase was detected in TEM, it can be concluded that most of the Zr incorporated into the CeO_2 phase and formed a $Zr_xCe_{1-x}O_2$ solid solution of cubic symmetry, where x should be equal to the actual Zr loading if no other Zr-containing phase coexisted in the system. The lattice constant of the solid solution decreased with increasing Zr loading. Figure 1(d) is an XRD pattern for ZrO_2/Al_2O_3 with no Ce. Only the γ-Al_2O_3 phase was detectable in the XRD pattern. Although Zr signals were detected easily by EDX in the TEM, most of the observed supported particles in this sample were found to be between 10 and 25 Å. This implies that the zirconia on the surface of γ-Al_2O_3 is highly dispersed or of poor crystallinity.

Three selected XRD patterns for steam-aged samples are shown in Fig. 2(a–c). After steam-aging at 1000°C, the cubic phase of the Ce–Zr oxide solid solution remained in the samples which contained Ce and Zr. At low Zr loading ($Zr \leq 150$ μmol/g-Al_2O_3, Ce 1500 μmol/g-Al_2O_3), only the cubic phase of the supported solid solution was detected as shown in Fig. 2(a). However, a new phase appeared in the samples with higher Zr loading ($Zr \geq 150$ μmol/g-Al_2O_3, Ce: 1500 μmol/g-Al_2O_3). New peaks labeled B′ were detected at the higher Zr loading, as shown in Fig. 2(b). With increasing Zr loading, the 2θ values of these peaks shifted toward those of tetragonal ZrO_2 (Fig. 2(c)). Figure 3 clearly shows the (111) peak of phase B shifting away from that of CeO_2, and the (111) peak of phase B′ shifting to that of ZrO_2 for a series of 6 samples also steam aged at 1000°C. Although the exact Zr concentrations, x in phase B ($Zr_xCe_{1-x}O_2$) and x' in phase B′ ($Zr_{x'}Ce_{1-x'}O_2$), are unknown, it is possible to estimate the Zr concentration in the solid solution phase from the lattice parameter. That discussion will be deferred to the next section of the paper.

The average particle sizes of fresh and steam-aged samples are shown plotted against Zr loading in Fig. 4. The full-width at half maxima of the (111) peaks of the cubic $Zr_xCe_{1-x}O_2$ phase were used for size calculation with the Scherrer equation. For TEM size measurement, Ce–Zr oxide particles in aged samples were identified using EDX and image contrast. It was found that both the Zr and Ce X-ray singles were always observed from each individual particle. This strongly suggests that the particles were solid solutions instead of separate Zr and Ce oxide particulates. Figure 5(a)

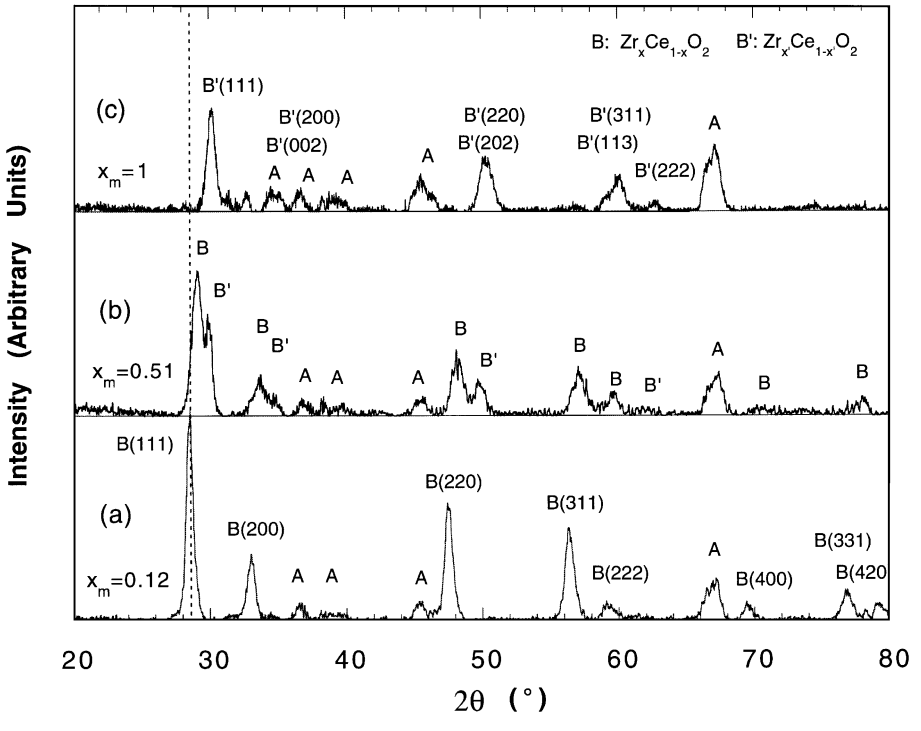

FIG. 1. XRD patterns for fresh $ZrO_2(x)$–$CeO_2(y)/Al_2O_3$ samples at various Zr loadings: (a) $x=0$, $y=1500$ μmol/g-Al_2O_3; (b) $x=300$ μmol/g-Al_2O_3, $y=1500$ μmol/g-Al_2O_3; (c) $x=1500$ μmol/g-Al_2O_3, $y=1500$ μmol/g-Al_2O_3; (d) $x=1500$ μmol/g-Al_2O_3, $y=0$.

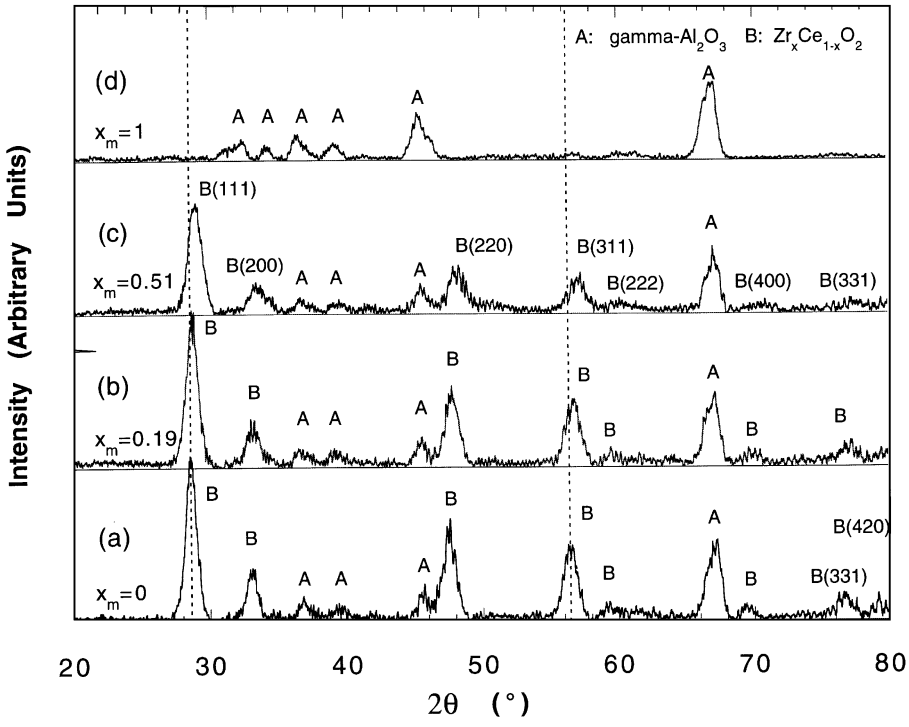

FIG. 2. XRD patterns for steam-aged $ZrO_2(x)$–$CeO_2(y)/Al_2O_3$ samples: (a) $x = 150$ μmol/g-Al_2O_3, $y = 1500$ μmol/g-Al_2O_3; (b) $x = 1500$ μmol/g-Al_2O_3, $y = 1500$ μmol/g-Al_2O_3; (c) $x = 1500$ μmol/g-Al_2O_3, $y = 0$.

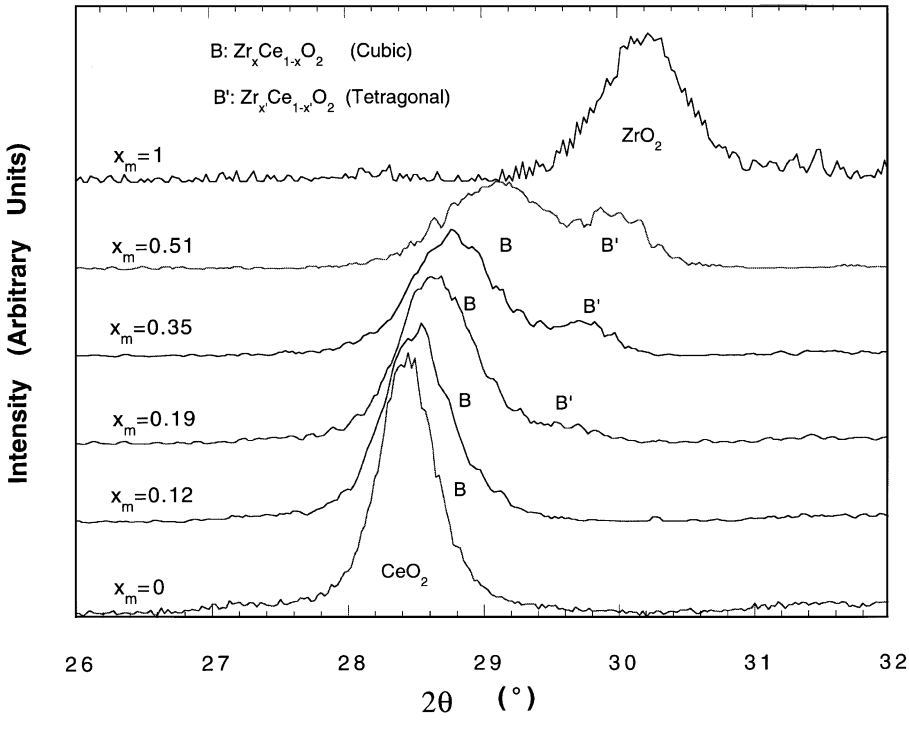

FIG. 3. (111) peak shifts at various zirconia loadings for a series of steam-aged samples.

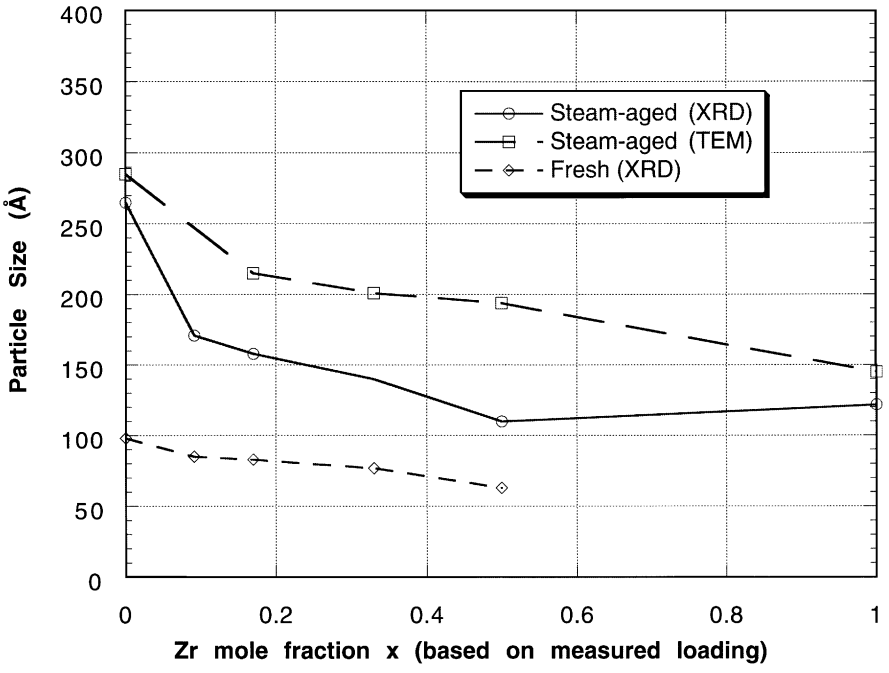

FIG. 4. Particle sizes of the supported cubic solid solution phase versus average Zr/Ce ratio.

is a TEM micrograph of fresh CeO_2(1500 μmol/g-Al_2O_3)-ZrO_2(1500 μmol/g-Al_2O_3). Although nanometer size particles are visible in the fresh samples, accurate statistical measurement could not be performed due to clustering of the particles and the inability of EDX to discriminate among the clustered ultrafine particles. Figures 5(b) and (c) are micrographs of steam-aged samples with and without zirconia, respectively. Ceria particles in Fig. 5(c) are considerably larger and better crystallized than Ce–Zr particles in Fig. 5(b). Both TEM and XRD results show decreasing sizes with increasing Zr loading, indicating that Zr addition improved the dispersion of the supported particles and retarded their sintering.

Zirconia also enhanced the stability of the support and supported phases. Figures 6(a) and (b) are XRD patterns of reduced samples with and without Zr, respectively. After high-temperature reduction, γ-Al_2O_3 reacted with the surface ceria and formed a $CeAlO_3$ phase as shown in Fig. 6(a). The average particle size of $CeAlO_3$ measured by XRD is 310 Å, which was considerably larger than the original γ-Al_2O_3 particle size of 140 Å. None of the XRD patterns of the samples containing both Ce and Zr showed the $CeAlO_3$ phase, and only one solid solution phase, the cubic phase, was observed.

4. DISCUSSION

Phases and Lattice Parameter

It is clear that the particulate phases in our samples are γ-Al_2O_3, $Zr_xCe_{1-x}O_2$ and $CeAlO_3$. However, the existence of atomically dispersed Zr and Ce oxide surface species cannot be excluded. The highly dispersed phases would not produce X-ray diffraction patterns, and they also would be difficult to detect by TEM. To determine if there are dispersed surface species, it is helpful to evaluate the difference between the Zr concentration in the particulate phase and the actual Zr loading. For the solid solution $Zr_xCe_{1-x}O_2$, the lattice parameter is partially determined by the Zr concentration x; the larger x, the smaller the lattice parameter.

Lattice parameters of the supported solid solutions versus measured Zr loading are shown in Fig. 7. Lattice parameters of the unsupported ceramic system $Zr_xCe_{1-x}O_2$ are also shown for reference. The reference data are from the JCPDS database (13). Significantly, the lattice parameters of the supported cubic phase were all larger than those of bulk solid solutions at corresponding Zr concentration, assuming complete incorporation of the Zr into the solid solution. If the change of the lattice parameter in the solid solution is determined by the Zr concentration, this observation suggests that the Zr concentration in the cubic phase of supported $Zr_xCe_{1-x}O_2$ is lower than the actual Zr loading. The excess Zr must exist in another phase. In the fresh, steam-aged, and reduced samples of low Zr loading, the only supported phase detected by XRD was the Ce–Zr oxide solid solution. Therefore the excess Zr is most likely present in a highly dispersed form on the surface of the γ-Al_2O_3 particles.

Comparing the lattice parameters of fresh, steam-aged and reduced samples at corresponding Zr loadings, it was found that the lattice parameters for the high-temperature

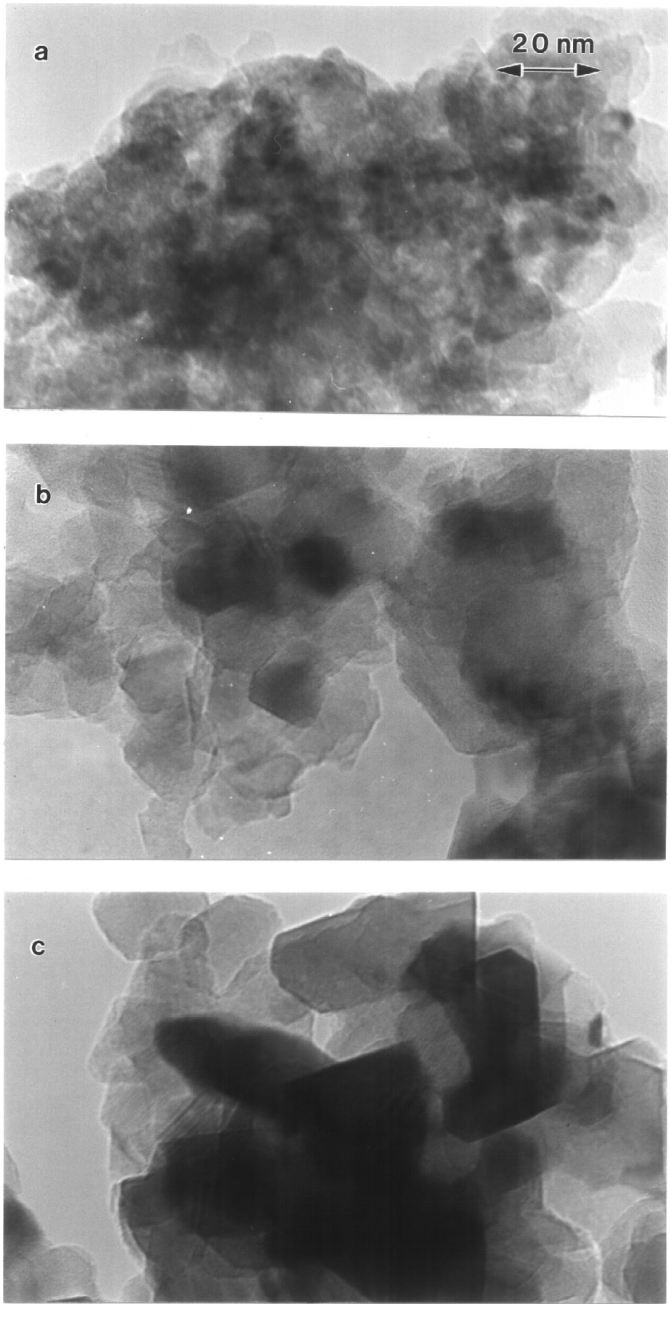

FIG. 5. TEM micrographs of: (a) fresh CeO_2(1500 μmol/g-Al_2O_3)-ZrO_2(1500 μmol/g-Al_2O_3)/Al_2O_3; (b) steam-aged CeO_2(1500 μmol/g-Al_2O_3)-ZrO_2(1500 μmol/g-Al_2O_3)/Al_2O_3; and (c) steam-aged CeO_2(1500 μmol/g-Al_2O_3)/Al_2O_3.

reduced samples are the smallest. This may indicate that reduction caused Zr in the dispersed phase to concentrate into to the particulate phase of the CeO_2-based solid solution since the Zr concentration x in the solid solution, inferred from the lattice constant, is close to the Zr loading. The fresh sample at high Zr loading (ZrO_2: 1500 μmol/g-Al_2O_3, CeO_2: 1500 μmol/g-Al_2O_3) has the largest lattice parameter, suggesting that more Zr was in the dispersed phase in fresh samples than in reduced and steam-aged samples. For most steam-aged samples, the lattice parameters are found to be larger than those of reduced and fresh samples. This may be explained by the growth of the second solid solution phase $Zr_{x'}Ce_{1-x'}O_2$ during steam-aging. As shown in Fig. 4, the solid solution B′ ($Zr_{x'}Ce_{1-x'}O_2$) is Zr-rich, and approaches tetragonal ZrO_2 as the Zr loading increases. Because of the coexistence of the Zr-rich solid solution B′, the Zr concentration in the cubic phase B is deficient from the actual loading, and the lattice parameter is therefore larger.

The source of the second solid solution phase B′ is not totally understood. It is possible that the dispersed Zr and Ce oxide surface species are mainly responsible for the phase B′. By comparing the XRD patterns of the Figs. 1(a) and (d), one can see that zirconia is much better dispersed than the ceria in the freshly prepared state. There must be more zirconia in a finely dispersed state than ceria. The dispersed surface Zr and Ce oxide species could sinter under an oxidizing atmosphere at high temperature to form the Zr-rich particulate phase B′. It is also possible that the $CeO_2 \cdot ZrO_2$ solid solution particles phase-separate under high-temperature steam ageing. The phase diagrams for bulk $CeO_2 \cdot ZrO_2$ show limited mutual solubility with two phase regions from 10 to 85 mol% Zr (14). The boundary between the cubic-monoclinic and cubic-tetragonal coexistence regions is at about 1000°C (1050 ± 50°C) (14) so that these results are not inconsistent with incomplete phase separation since the phases have variable composition as evidenced by their varying lattice constant.

Stabilizing Effect

It has been reported (15) that a large fraction of highly dispersed ceria on γ-Al_2O_3 is in a +3 state and that these Ce^{+3} ions can be converted to $CeAlO_3$ upon reduction. As shown in Fig. 5, our XRD data confirmed this observation. For the sake of stability, a highly dispersed CeO_2 phase may be undesirable because of the ease of $CeAlO_3$ formation. On the other hand, if highly dispersed CeO_2 can be prevented from reacting with γ-Al_2O_3, it should favor OSC. Graham *et al.* (16) reported that the incorporation of La^{3+} into the Al_2O_3 before CeO_2 is added may prevent reaction between CeO_2 and Al_2O_3, and result in a higher CeO_2 dispersion and greater range of reversibility of the Ce^{+4}/Ce^{+3} redox reaction. In our study, the highly dispersed zirconia appeared to protect CeO_2 from reaction with γ-Al_2O_3. The dispersed ZrO_2 can play this role by reacting more easily with dispersed CeO_2 and/or covering the surface of alumina.

Particle Sizes by XRD and TEM

Although both XRD and TEM showed decreasing particle size with increasing zirconia loading, the

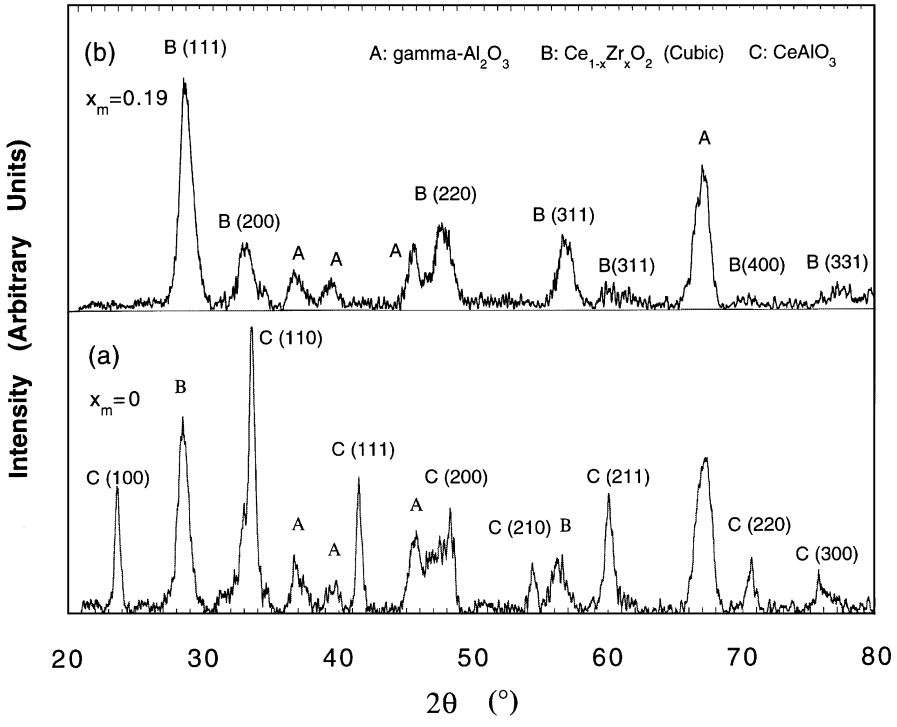

FIG. 6. XRD patterns for reduced $ZrO_2(x)$–$CeO_2(y)/Al_2O_3$ samples: (a) $x = 0$ μmol/g-Al_2O_3, $y = 1500$ μmol/g-Al_2O_3; (b) $x = 300$ μmol/g-Al_2O_3, $y = 1500$ μmol/g-Al_2O_3.

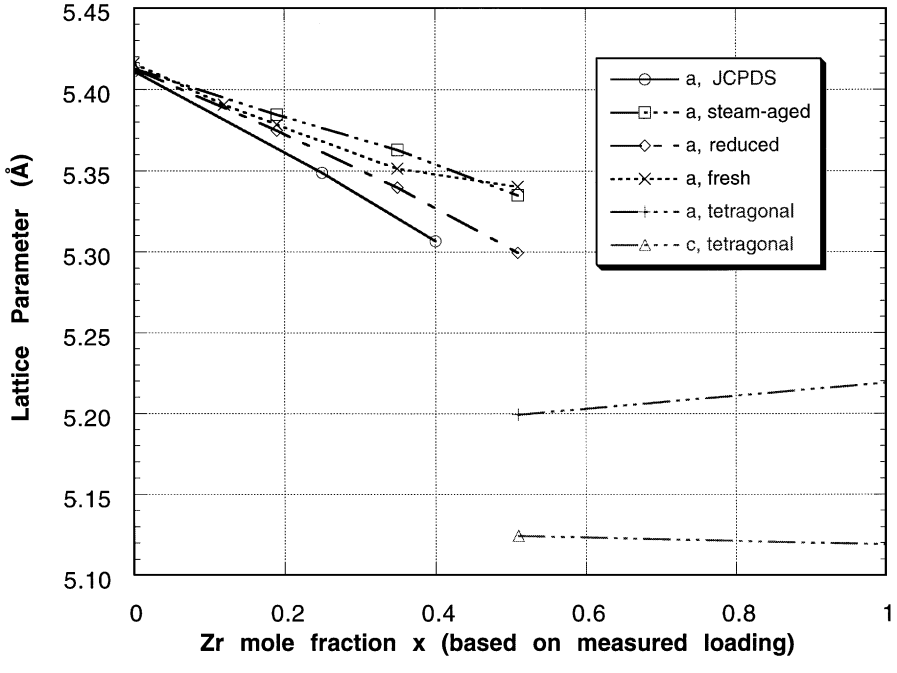

FIG. 7. Lattice parameters (**a** for cubic phases, **a** and **c** for tetragonal phases) of the supported solid solutions as a function of Zr concentration. The lines for the tetragonal phase are an extrapolation to the tetragonal-ZrO_2 lattice constants since no samples in the range $0.51 < x < 1.0$ were examined.

volume-weighted average particle sizes calculated from the TEM data were consistently larger than those calculated from the Scherrer equation. This may be due to systematic reasons. The particle sizes from the Scherrer equation are determined from line broadening, which is dependent not only on the size of the coherent scattering domains but also on the disorder (compositional and geometric) of the crystal particles. The particle size effects give rise to an order independent line broadening. Both compositional and geometric inhomogeneity, i.e., lattice strain, give rise to the same form of order dependent line broadening. In our samples, compositional fluctuation existed (this must be true, otherwise we would not have seen the phases B and B′ of different chemical composition coexisting in thermally aged samples). So it is plausible to suggest that the Zr concentration in each particle may not be exactly the same, and therefore the lattice parameter may be slightly different from particle to particle. The fluctuation from the average lattice parameter will cause an apparent broadening in addition to the size-induced broadening. Since it is not possible to differentiate or separate this effect from strain induced broadening, it is possible that there is also a strain component in the measured line width. Statistically, the higher the Zr loading ($\leq$50%), the greater the opportunity for compositional fluctuation. We see the greatest difference between TEM and XRD results as the zirconia loading increased to 50%. In summary, when measuring the particle size of a complex particle system, the use of multiple methods can give complementary and more complete results.

5. CONCLUSIONS

XRD and TEM have been employed to study the supported CeO_2–ZrO_2/Al_2O_3 system. A particulate solid solution phase $Zr_xCe_{1-x}O_2$ of cubic symmetry was identified in the fresh samples at Zr loading $x = 0$ to 0.5. From analysis of the change in lattice parameter as a function of Zr loading, it is suggested that the actual concentration of Zr in the particulate phase is smaller than the Zr loading. This, coupled with the fact that no particulate Zr containing phase was observed in TEM, further implies that the excess zirconia exists in a highly dispersed state which was undetectable by XRD. In steam-aged samples, two solid solution phases were found. One was the original CeO_2 based Ce–Zr oxide solid solution of cubic symmetry. The other was also a Ce–Zr oxide solid solution, but it has a higher Zr concentration relative to the original cubic phase, and the structure approaches that of tetragonal ZrO_2 as the Zr loading increased. Sintering of the highly dispersed zirconia may be responsible for the growth of the second solid-solution phase. The determination of how these two solid-solution phases contribute to the OSC, respectively, requires further investigation.

Our experiments confirmed that dispersed CeO_2 could react with the alumina support to form $CeAlO_3$ upon reduction. However, the $CeAlO_3$ phase was not detected in any reduced samples that contained Zr. This observation implies that highly dispersed zirconia can prevent dispersed CeO_2 from reacting with the supporting Al_2O_3.

The particle sizes of various phases were measured by XRD and TEM. The average particle size of the CeO_2 based Ce–Zr oxide solid solution decreased with increasing zirconia loading. A discrepancy observed between XRD and TEM determination of particle sizes may be due to the compositional fluctuation in the supported particles. These compositional fluctuation resulted in additional XRD peak profile broadening and smaller calculated particle sizes.

ACKNOWLEDGMENTS

The authors thank K. A. Laframboise for assistance in sample preparation and R. O. Carter III and George Graham for helpful discussions and reading this manuscript.

REFERENCES

1. Summers, C., and Ausen, S. A., *J. Catal.* **58**, 131 (1979).
2. Harrison, B., Dwiwell, A. F., and Hallet, C., *Plat. Met. Rev.* **32**, 73 (1988).
3. Blackenburg, K. J., and Datye, A. K., *J. Catal.* **128**, 1 (1991).
4. Loof, P., Kasemo, B., and Keck, K. E., *J. Catal.* **118**, 339 (1989).
5. Murota, T., Hasegawa, T., and Aozasa, S., *J. Alloys Compounds* **193**, 298 (1993).
6. Murrell, L. L., and Tauster, S. J., *in* "Catalysis and Automotive Pollution Controll II" (A. Crucq, Ed.), p. 547. Elsevier, Amsterdam, 1991.
7. Duwez, P., and Odell, F., *J. Am. Ceram. Soc.* **33**, 274 (1950).
8. Tani, E., Yoshimura, M., and Somiya, S., *J. Am. Ceram. Soc.* **66**, 506 (1983).
9. Meriani, S., and Spinolo, G., *Powder Diffr.* **2**, 255 (1987).
10. Meriani, S., *Mat. Sci. Eng.* **A109**, 121 (1989).
11. Warren, B. E., "X-Ray Diffraction," p. 253. Addison-Wesley, Reading, MA, 1969.
12. Yao, M. H., Liu, D. R., Baird, R., Usmen, R. K., and McCabe, R. W., *in* "Proceedings 52nd Annual Meeting of the MSA (1994)," p. 776. San Francisco Press, San Francisco, 1994.
13. JCPDS (Card No. 43-1002 for $x = 0$, 28-0271 for $x = 0.25$, and 38-1439 for $x = 0.4$), International Center for Diffraction Data, Newton Square Corporate Campus, 12 Campus Blvd., Newton Square, PA 19073.
14. Tani, E., Yoshimura, M., and Somiya, S., *J. Am. Cer. Soc.* **66**, 506 (1983).
15. Shyu, J. Z., Weber, W. H., and Gandhi, H. S., *J. Phys. Chem.* **92**, 4964 (1988).
16. Graham, G. W., Schmitz, P. J., Usmen, R. K., and McCabe, R. W., *Catal. Lett.* **17**, 175 (1993).